Materials Horizons

ROYAL SOCIETY OF CHEMISTRY

COMMUNICATION

View Article Online
View Journal | View Issue

Cite this: *Mater. Horiz.*, 2023, **10**, 3090

Received 19th March 2023,
Accepted 12th May 2023

DOI: 10.1039/d3mh00418j

rsc.li/materials-horizons

Tunable control of the performance of aqueous-based electrochemical devices by post-polymerization functionalization†

Shengyu Cong,‡[a] Junxin Chen,‡[a] Bowen Ding,[b] Liuyuan Lan,[a] Yazhou Wang,[a] Chaoyue Chen,[a] Zhengke Li,[a] Martin Heeney*[bc] and Wan Yue *[a]

Functionalized polymeric mixed ionic–electronic conductors (PMIECs) are highly desired for the development of electrochemical applications, yet are hindered by the limited conventional synthesis techniques. Here, we propose a "graft-onto-polymer" synthesis strategy by post-polymerization functionalization (GOP-PPF) to prepare a family of PMIECs sharing the same backbone while functionalized with varying ethylene glycol (EG) compositions (two, four, and six EG repeating units). Unlike the typical procedure, GOP-PPF uses a nucleophilic aromatic substitution reaction for the facile and versatile attachment of functional units to a pre-synthesized conjugated-polymer precursor. Importantly, these redox-active PMIECs are investigated as a platform for energy storage devices and organic electrochemical transistors (OECTs) in aqueous media. The ion diffusivity, charge mobility and charge-storage capacity can be significantly improved by optimizing the EG composition. Specifically, g2T2-gBT6 containing the highest EG density gives the highest charge-storage capacity exceeding 180 F g^{-1} among the polymer series, resulting from the improved ion diffusivity. Moreover, g2T2-gBT4 with four EG repeating units exhibits a superior performance compared to its two analogues in OECTs, associated with a high μC^* up to 359 F V^{-1} cm^{-1} s^{-1}, owing to the optimal balance between ionic–electronic coupling and charge mobility. Through the GOP-PPF, PMIECs can be tailored to access desirable performance metrics at the molecular level.

New concepts

Functionalized polymeric mixed ionic–electronic conductors (PMIECs) are crucial for a host of applications underpinning societal needs from energy storage to health technologies. However, functional properties required for these application domains face synthetic challenges to being conveyed onto π-backbones and thus combined with efficient mixed conduction. Here, we present the very first bottom-up approach to synthesize a series of functionalized PMIECs with comparable molecular weights based on a "graft-onto-polymer" synthesis strategy by post-polymerization functionalization (GOP-PPF). Notably, GOP-PPF uses a nucleophilic aromatic substitution reaction for the facile attachment of functional units to a pre-synthesized conjugated-polymer precursor. Unlike the typical procedure, such GOP-PPF can largely simplify time-consuming multiple steps involving diverse side chain synthesis. In particular, the ion diffusivity, charge mobility and charge-storage capacity can be significantly improved by a rational functionalization design. Moreover, GOP-PPF provides only one variation to establish accurate structure–property relationships. Overall, this work provides design guidelines to approach the functionalized synthesis of PMIECs and offer new opportunities to explore their untapped potential.

1. Introduction

Polymeric mixed ionic–electronic conductors (PMIECs), which can simultaneously transport and couple ionic and electronic charges, are crucial for a host of technological developments for bioelectronics,[1] optoelectronics[2] and energy storage devices.[3] PMIECs are often functionalized conjugated polymers (CPs),[4,5] composed of a delocalised backbone, which supports the electronic charge transport, while appropriate side chains allow the ionic transport.[6,7] Additionally, the ready variability of the backbone structure of CPs allows fine tuning of their properties to maximize performance in various electrochemical devices, such as the organic electrochemical transistor (OECT)[8] and energy storage devices.[9] For all of these applications, the interaction of the polymer with aqueous electrolytes is a critical parameter.[10] Ions must enter and exit the film to balance

[a] *Guangzhou Key Laboratory of Flexible Electronic Materials and Wearable Devices, School of Materials Science and Engineering, Sun Yat-sen University, Guangzhou 510275, People's Republic of China. E-mail: yuew5@mail.sysu.edu.cn*
[b] *Department of Chemistry and Centre for Processable Electronics, Imperial College London, Molecular Sciences Research Hub (White City Campus), 80 Wood Lane Shepherd's Bush, London W12 0BZ, UK. E-mail: martin.heeney@kaust.edu.sa*
[c] *KAUST Solar Center (KSC), Physical Science and Engineering Division (PSE), King Abdullah University of Science and Technology (KAUST), Thuwal, 23955–6900, Saudi Arabia*

† Electronic supplementary information (ESI) available. See DOI: https://doi.org/10.1039/d3mh00418j

‡ S. Cong and J. Chen contributed equally to this work.

charges introduced by the redox chemistry of the conjugated backbone.[11]

However, classical CPs are often hydrophobic as a result of their alkyl side chains and aromatic building blocks.[12] In order to promote the ionic conductivity in aqueous electrolytes, the polarity of the CPs can be modulated to increase their hydrophilic feature.[13] One common approach is to introduce highly hydrophilic ethylene glycol (EG) or its derivates as side chains, which facilitates ionic species transport.[14,15] Nonetheless, several studies presented that excessive EG density will disrupt the favorable molecular packing and bring a loss of structural integrity, which results in low charge mobility.[16,17] Besides, the overlong EG side chain will lead to a decrease in the electroactive fraction of the polymers, and thus may cause a decrease in charging capability.[18] Consequently, EG composition optimization is crucial for the design of CPs as PMIECs operating in aqueous electrolyte.

At present, the synthetic routes towards EG functionalized PMIECs involve synthesizing monomers with the EG side chain first, followed by subsequent polymerization with a variety of building blocks to form the glycolated target copolymers.[19,20] However, such synthetic routes have some drawbacks and processing challenges (see Scheme 1A): (1) challenging monomer purification and low yield have been reported for long EG lengths, restricting the hydrophilicity tunability;[21] (2) to investigate the impact of EG composition, time-consuming multiple steps are usually involved in the synthesis of monomers with variable EG length;[20,22,23] (3) when preparing a series of co-polymers from monomers with different EG compositions, it is often difficult to ensure polymers of comparable molecular weights due to differing monomer purities and solubilities, and the variability of the step-growth polymerization.[24,25] Therefore, the EG functionalized CPs from different batches likely differ in the molecular weights and EG composition, which makes it difficult to decouple the two effects.[25] Although the chain-growth Kumada catalyst transfer polymerization was successfully applied to synthesize EG-containing polythiophenes where the molecular weights are comparable,[4,26,27] this is harder for typical step growth polymerizations like Stille or Suzuki. Therefore, hindered by the limited functionalization methods offered by conventional synthesis techniques, the absence of an effective synthesis strategy poses a major obstacle to taking

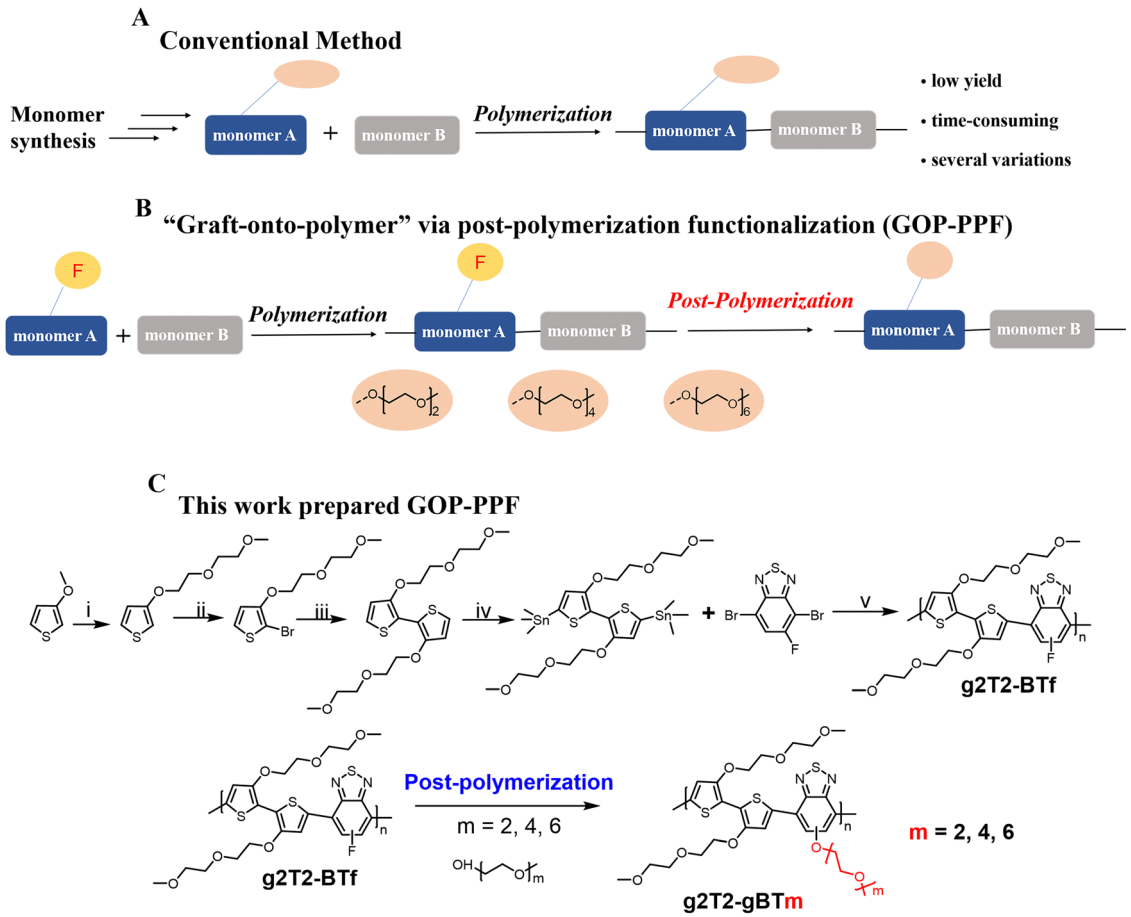

Scheme 1 (A) Conventional approach of pre-polymerization side-chain functionalization on conjugated polymers, and the associated limitations. (B) "Graft-onto-polymer" synthesis strategy by post-polymerization functionalization (**GOP-PPF**) using nucleophilic aromatic substitution (S_NAr) reaction to functionalize the side chains of the conjugated polymers. (C) EG functionalized PMIECs synthesized by post-polymerization functionalization. Reaction conditions: (i) toluene, *p*-TsOH, 2-(2-methoxyethoxy)ethanol, 110 °C; (ii) NBS, anhydrous DCM, 0 °C, 2 h; (iii) $Ni(COD)_2$, COD, BPy, THF; (iv) *n*-BuLi, Me_3SnCl, THF, −78 °C; (v) $Pd_2(dba)_3$, P(*o*-tol)$_3$, toluene, 110 °C, 24 h. Post-polymerization condition: NaOH, chlorobenzene:DMF (3 : 1), 120 °C, 48 h.

advantage of the unique properties of PMIECs to benefit the development of electrochemical devices.

Post-polymerization functionalization *via* nucleophilic aromatic substitution (S_NAr) reaction can overcome the difficulties mentioned above. In this approach, functional groups are added to a preformed polymer by chemical reaction.[28,29] High yield reactions are required, otherwise the post-polymerization approach can afford complex mixtures, but it can also allow the introduction of groups which would otherwise not survive the polymerization conditions.[30–32] More importantly, as post-polymerization functionalization originates from the same batch of precursor polymer, the resulting functionalized polymers should have identical chain length, minimizing the impact of molecular weight variation on the properties and providing only one variable to access accurate comparisons of device performances based on the target copolymers.[33,34]

Here, to unlock a broad range of desired functionalities for conjugated polymers, we propose a ''graft-onto-polymer'' synthesis strategy by post-polymerization functionalization for conjugated polymers, which uses a nucleophilic aromatic substitution reaction for the facile and versatile attachment of functional units to a pre-synthesized conjugated-polymer precursor (Scheme 1B). In particular, we employ this approach to modify the EG composition on the π-conjugated backbones and investigate the resulting doping on the coupling between ionic and electronic species along the polymer backbone in aqueous media. Such an approach can directly functionalize the backbone of a CP by nucleophilic aromatic substitution (S_NAr) reaction.[34] Our polymeric framework is based on an alternating bithiophene and 5-fluoro-2,1,3-benzothiadiazole (**BTf**) backbone, which as previously reported has a coplanar backbone conformation benefitting charge transport.[35] In addition, we have previously demonstrated that the fluorine substituent of **BTf** can be substituted by various nucleophiles in the presence of base, leading to a facile route for the introduction of EG of varying length, specifically 2, 4 and 6 repeating units[34,36] (Scheme 1C). The varying EG composition enables tuning of the PMIECs' hydrophilicity, charge–discharge kinetics, ionic–electronic coupling and charge mobility.[37,38]

Overall, by systemically comparing a family of PMIECs' redox behavior and electrochemical properties in energy-storage and OECTs, we elucidated the role of the EG composition in electrochemical performance in aqueous media. In energy storage, **g2T2-gBT6** containing the highest EG density gave the highest charge-storage capacity exceeding 180 F g^{-1} among the polymer series, resulting from the improved ion diffusivity. For OECTs, **g2T2-gBT4** with four EG repeating units exhibited a superior performance than its two analogues, associated with a high μC^* up to 359 F V^{-1} cm^{-1} s^{-1} and an OECT charge mobility of 0.99 cm^2 V^{-1} s^{-1}, owing to its optimal balance between ionic and electronic transport. Additionally, inferior charge-storage capacity and OECT performance were both found in **g2T2-gBT2**, which is due to the combined effects of low degree of swelling and mixed ionic–electronic conduction as it has the lowest EG density. Moreover, the ''graft-onto-polymer'' synthesis strategy by post-polymerization functionalization (**GOP-PPF**) proposed in this work shows great potential in functionalized PMIEC synthesis, bringing reliable establishment of structure–property relationships, and largely enriching the protocols to optimize the performance of aqueous-based electrochemical devices.

2. Results and discussion

2.1 The EG functionalized PMIEC synthesis

The family of PMIECs synthesized by post-polymerization functionalization are illustrated in Scheme 1C and the synthetic procedures are presented in Scheme S1 and S2 (ESI†). First, 3-methoxythiophene was treated in turn with 2-(2-methoxyethoxy)-ethanol and n-bromosuccinimide to give 2-bromo-3-[2-(2-methoxyethoxy)ethoxy]thiophene in a moderate yield. This was dimerised by the action of bis(1,5-cyclooctadiene)nickel (0) to afford glycolated bithiophene. This was then stannylated by dilithiation with *n*-BuLi, followed by trapping with trimethyltin chloride. Commercially available **BTf** was polymerized with the resulting stannylated bithiophene under typical Stille conditions to give **g2T2-BTf**. Under nucleophilic aromatic substitution conditions,[34] **g2T2-BTf** was amenable to direct displacement of the fluorine atom by grafting a series of EG (x = 2, 4, 6) to give **g2T2-gBT2**, **g2T2-gBT4** and **g2T2-gBT6**. The successful synthesis of polymeric materials by post-polymerization functionalization was confirmed by ^{1}H-NMR and ^{19}F-NMR. It is worth noting that these PMIECs are insoluble in water-based electrolytes, which allows the characterization of their redox activity in aqueous electrolytes. Importantly, the three PMIECs synthesized by post-polymerization functionalization all originate from the same batch of **g2T2-BTf**, which indicates that they share similar molecular weights. The comparable molecular weights were confirmed by gel permeation chromatography (GPC) using DMF as the eluent (Fig. S13 and Table S1, ESI†). The number average molecular weight (M_n) and dispersity of **g2T2-BTf** were 9.9 kg mol^{-1} and 1.17, respectively. As expected, the EG functionalized PMIECs present comparable molecular weights (10.1 to 10.5 kg mol^{-1}) and dispersity (1.18–1.20), which enables the resulting PMIECs to only differ in the length of their attached functional side chains.

2.2 Optical and electronic properties

The optical properties of the PMIECs were measured by UV-vis-NIR absorption in solution (chloroform) (Fig. S14, ESI†) and films (Fig. 1a). Both in films and solution, all the absorption spectra exhibited similar absorption profiles with a dual-band absorption. A high energy band from 360–510 nm is attributed to the π–π* transition and a low-energy band from 510–1000 nm originates from an intramolecular charge transfer (ICT).[39] In solution, an absorption maximum (λ_{max}) at 640 (395) nm, 725 (422), 727 (423) and 728 (424) nm was observed for **g2T2-BTf**, **g2T2-gBT2**, **g2T2-gBT4** and **g2T2-gBT6**, respectively. When the electron-withdrawing fluoride atom was substituted by an electron-donating ether group, a red-shift for both bands was found in all examples. Additionally, the intensity of the ICT band of EG functionalized PMIECs slightly decreased with respect to the high energy band, which results from the

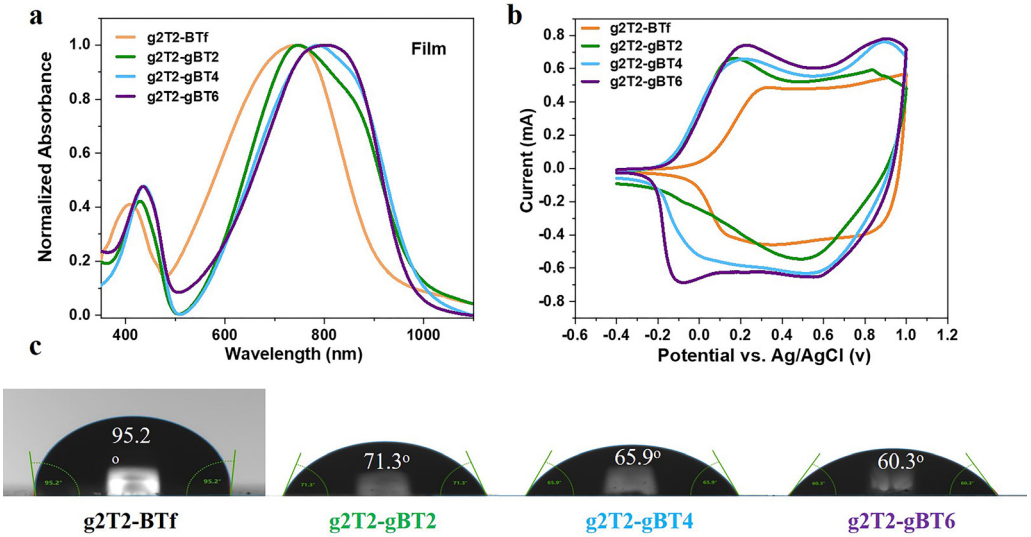

Fig. 1 (a) Normalized UV-vis-NIR absorption spectra in films and (b) cyclic voltammograms of the polymer films in 0.1 M tetrabutylammonium hexafluorophosphate (n-Bu_4NPF_6) acetonitrile solution at a scan rate of 50 mV s^{-1}, using Ag/AgCl as a reference electrode. (c) Contact angle measurements.

weakening of the electron-accepting ability of the benzothiadiazole.[36,40]

For the EG functionalized PMIECs, little change in the λ_{max} or spectrum shape was observed when increasing the EG length, which is consistent with previous reports.[36] Interestingly, a shoulder found around 800 in chloroform for all polymers was attributed to the aggregation of the conjugated chains in solution.[41] By monitoring the film spectra, the λ_{max} of the PMIECs all exhibited an apparent red-shift compared with their solution absorption, indicating enhanced molecular packing and stronger aggregation in the film state.[42] Based on the film absorption onsets, the optical bandgaps (E_g^{opt}) are estimated to be 1.27 ± 0.2 eV for EG functionalized PMIECs, smaller than 1.33 eV for **g2T2-BTf**. The larger bandgap of **g2T2-BTf** is attributed to the relatively stronger ICT character.[43] Noticeably, variations in EG composition present little change on PMIECs' electronic properties.

The electrochemical properties of PMIECs were measured by cyclic voltammetry (CV) in 0.1 M n-Bu_4NPF_6 in dry acetonitrile using Ag/AgCl as a reference electrode. As displayed in Fig. 1b, the highest occupied molecular orbital (HOMO) energy levels were estimated based on the oxidative onset potentials relative to the ferrocene/ferrocenium (Fc/Fc^+) redox couple as an external standard. Although the EG density on benzothiadiazole is variable, the EG functionalized PMIECs exhibited almost the same energy levels. The lowest unoccupied molecular orbital (LUMO) energy levels/HOMO energy levels (E_{LUMO}/E_{HOMO}) were found to be −3.13/−4.46 eV, −3.04/−4.31 eV, −3.04/−4.30 eV and −3.02/−4.31 eV for **g2T2-BTf**, **g2T2-gBT2**, **g2T2-gBT4** and **g2T2-gBT6**, respectively. The **g2T2-BTf** presented deeper lying E_{LUMO}/E_{HOMO} with respect to the EG functionalized PMIECs, resulting from the strong electron-withdrawing character of the fluorine atom.[43] The EG functionalized PMIECs gave E_{HOMO} around −4.31 eV, indicating that they are prone to be electrochemically doped in an aqueous electrolyte.[17] From the data in Table 1, the energetics of PMIECs remained constant even when grafting different lengths of EG side chains, demonstrating that the side chain composition has little impact on the PMIECs' electronic properties, which is in accordance with the optical measurement. Furthermore, the hydrophilicity was gradually raised by grafting longer EG side chains, which was supported by the contact angle measurement in Fig. 1c. The contact angle was 95.2° (±1.8), 71.3° (±1.4), 65.9° (±1.4) and 60.3° (±1.3) for **g2T2-BTf**, **g2T2-gBT2**, **g2T2-gBT4** and **g2T2-gBT6**, respectively.

Table 1 Optical and electronic properties

Polymers	$\lambda_{Solution}$ [a] [nm]	λ_{Film} [b] [nm]	E_{HOMO} [c] [eV]	E_{LUMO} [d] [eV]	E_g^{opt} [e] [eV]
g2T2-BTf	395, 640	410, 743	−4.46	−3.13	1.33
g2T2-gBT2	422,725	428,748	−4.31	−3.04	1.27
g2T2-gBT4	423,727	434,788	−4.30	−3.04	1.26
g2T2-gBT6	424,728	436,802	−4.31	−3.02	1.29

[a] Chloroform. [b] Films. [c] E_{HOMO} was determined by the equation $E_{HOMO} = -[4.8 + E_{ox(onset)} - E_{FC}]$ eV, the E_{FC} is 0.38 eV when Fc/Fc^+ as an external standard. [d] $E_{LUMO} = E_{HOMO} + E_g^{opt}$. [e] Derived from the absorption onset of polymer film ($E_g^{opt} = 1240/\lambda_{onset}$).

2.3 Electrochemical charging properties in aqueous media

To investigate the relationship between the varying EG composition and electrochemical redox behavior in aqueous media, CV measurements were conducted in a 0.1 M aqueous NaCl solution between −0.3 V and 0.7 V *vs* Ag/AgCl. As illustrated in Fig. 2, the potential for the oxidation onset in the aqueous electrolyte is −0.11 ± 0.01 V for three PMIECs. It is notable that the overall CV current increases in the following order: **g2T2-gBT2** < **g2T2-gBT4** < **g2T2-gBT6**. This is in contrast to the electroactive mass of the PMIECs, *i.e.* the mass percentages

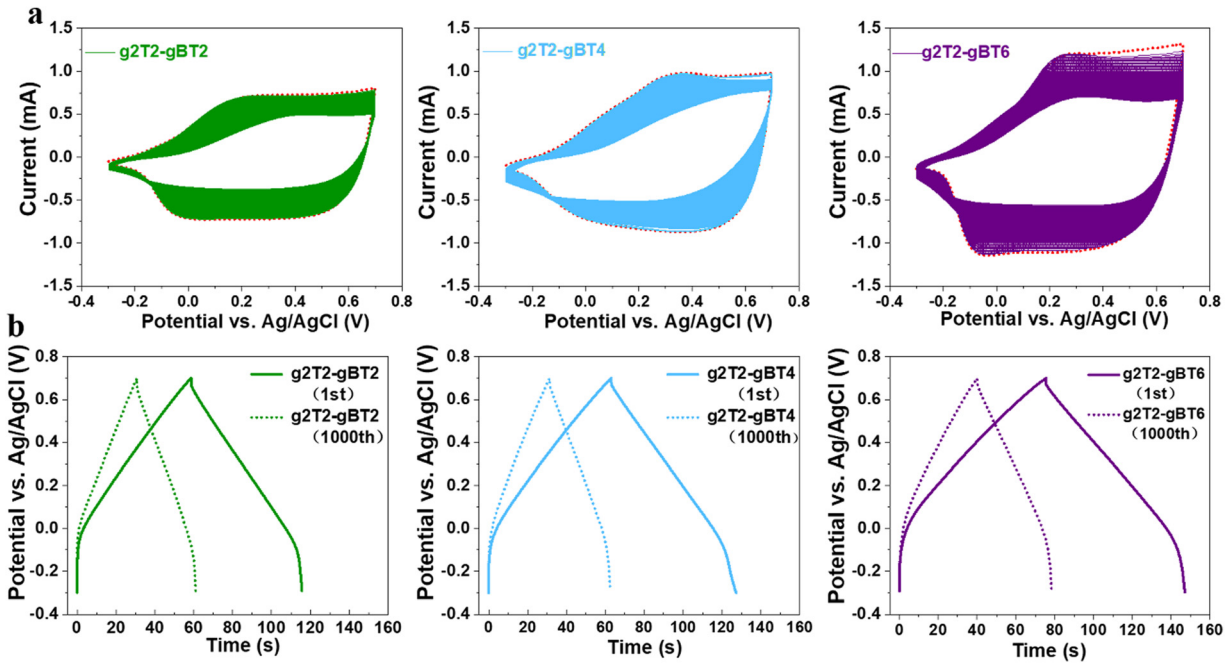

Fig. 2 (a) CV measurements of PMIECs in 0.1 M aqueous NaCl solution from −0.3 V to 0.7 V at a scan rate of 50 mV s^{-1} with low O_2 concentration (1000 cycles). The red circle represents the 1st cycle. (b) Galvanostatic charge–discharge plots recorded at 1.0 A g^{-1}.

of the conjugated backbone relative to the whole polymer, which were 46%, 40%, and 36% for **g2T2-gBT2**, **g2T2-gBT4** and **g2T2-gBT6**, respectively. With the greatest relative electroactive mass, **g2T2-gBT2** might be expected to provide the highest capacity, but this is not the case. The increasing energy-storage capacity with EG density thus indicates a positive impact of the EG side chains on the π-backbone doping.

As illustrated in Fig. 2a, varied differences in current density between the 1st and 1000th CV scan were observed. Upon continuous charging of the polymer films up to 1000 cycles, the three PMIECs exhibited similar electrochemical stability, retaining 55% ± 3% of the initial capacity. The gravimetric capacitance (C_g) is an important parameter for quantifying charge capacity of polymer electrodes, which can be obtained from CV recorded at 50 mV s^{-1} by integrating the current from −0.3 V to 0.7 V and normalizing for polymer mass. According to eqn (1):[44]

$$C_g = \frac{A}{\Delta V \times \left(\frac{\partial V}{\partial t}\right) \times m} \quad (1)$$

where A is the area under the CV curve, ΔV illustrates the voltage window (1.0 V in this case). $\frac{\partial V}{\partial t}$ is the scan rate and m represents the mass of the polymer. The C_g in 0.1 M aqueous NaCl solution was calculated as 113 F g^{-1} for **g2T2-gBT2**, 134 F g^{-1} for **g2T2-gBT4**, and 169 F g^{-1} for **g2T2-gBT6**. Note that the C_g calculation came from the first CV cycle. Apparently, gravimetric capacitance benefits from increasing the EG length. Furthermore, the galvanostatic charge–discharge (GCD) measurement for PMIECs recorded at 1 A g^{-1} was displayed in Fig. 2b. Follow eqn 2:[45]

$$C_s = \frac{2i_m \int^{V} dt}{V^2 \Big|_{V_i}^{V_f}} \quad (2)$$

where C_s represents the specific capacitance, $i_m \int^{V} dt$ depicts the current integral area and the current density (i_m) is 1.0 A g^{-1}. V_i is the initial voltage (−0.3 V) and the finished voltage is V_f (0.7 V), and then the voltage window square (absolute value) is 1.00 V^2. Substituting these values into eqn (2) gives a specific capacitance of 183 F g^{-1} for **g2T2-gBT6**, which is the highest value among the three PMIECs. Besides, the specific capacitance is 152 F g^{-1} for **g2T2-gBT4** and 140 F g^{-1} for **g2T2-gBT2**, which is consistent with the results from CV measurements. Similarly, GCD measurements support that higher specific capacitance was achieved by higher EG density. In addition, after 1000 cycles, the GCD measurement was carried out again. A specific capacitance of 74 F g^{-1}, 77 F g^{-1} and 97 F g^{-1} was obtained for **g2T2-gBT2**, **g2T2-gBT4** and **g2T2-gBT6**, respectively, which was in accordance with stability measurement around 55% after the 1000th cycle by CV. Both the CV and GCD measurements support that the storage capacity of the polymer electrode can be facilely tailored *via* EG composition modification by such post-polymerization functionalization.

The ability for these PMIECs to function as polymer-based electrodes in aqueous NaCl solution is attributed to doping of the π-backbone by chloride ions. As the **g2T2-gBT6** presented the superior storage capacity than its two analogues, we hypothesized that increasing EG content likely contributes to enhancing the doping of the conjugated backbone, enabling

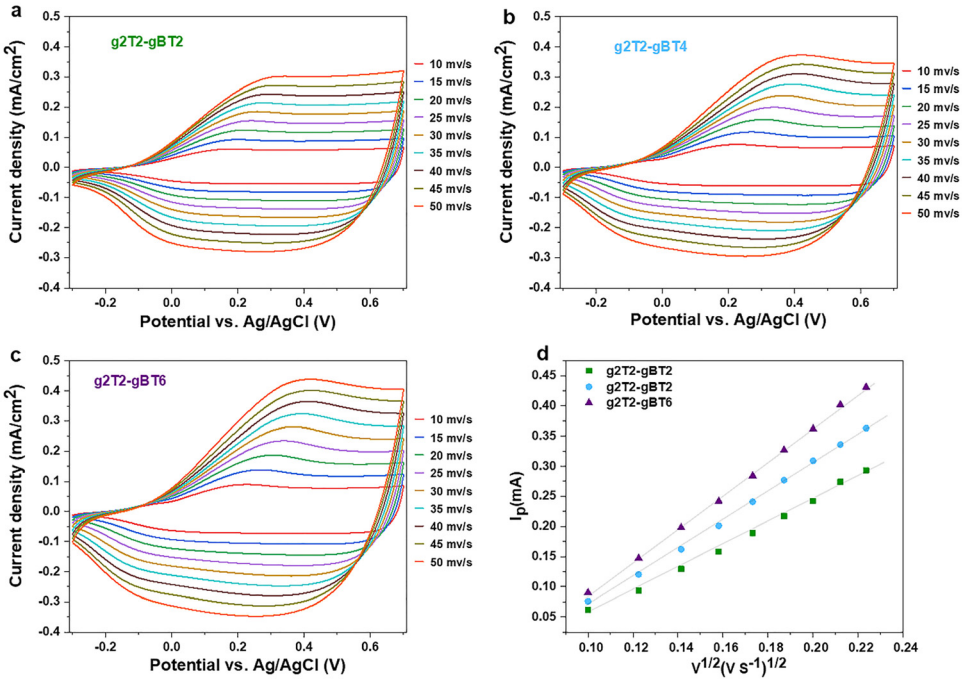

Fig. 3 (a–c) CV measurements of **g2T2-gBT2**, **g2T2-gBT4** and **g2T2-gBT6** in 0.1 M aqueous NaCl solution from −0.3 V to 0.7 V at a series of scan rates with low O_2 concentration; (d) peak currents against the square roots of the scan rates.

faster redox kinetics and better performance for the polymer electrodes.[9] To support this speculation, CV measurements of copolymers in deoxygenated 0.1 M aqueous NaCl solution were performed from −0.3 V to 0.7 V at a series of scan rates (Fig. 3a–c). A linear trend of relationship between current intensity and square root of scan rate was found in all three PMIECs, which suggests a diffusion-controlled mechanism of oxidation/reduction reactions (Fig. 3d).[46] According to the Randles–Sevcik equation for a reversible electrochemical process, the $I_p(v^{1/2})$ relationship can be described as eqn (3):[47]

$$I_P = 0.4463\left(\frac{n^3F^3}{RT}vD\right)^{1/2}AC \quad (3)$$

in which A is the polymer electrode's electrochemically active surface area (2.85 cm^2 in this case), ν is the scan rate (V s^{-1}), n is the number of electrons involved during the electrochemical process, F is Faraday's constant (C mol^{-1}), R is the gas constant (J (mol K)$^{-1}$), T is the absolute temperature (298.15 K), C is the molar concentration of chloride ions in NaCl solution (0.1 mol cm^{-3}) and D is the diffusion coefficient of chloride ions. Based on eqn (3), the D_{Cl^-} is calculated with a value of 3.43 × 10^{-10} cm^2 s^{-1}, 4.62 × 10^{-10} cm^2 s^{-1} and 6.12 × 10^{-10} cm^2 s^{-1} for **g2T2-gBT2**, **g2T2-gBT4** and **g2T2-gBT6**, respectively. Apparently, the higher EG density contributes to the electrochemical doping of the π-backbone, resulting from the improvement in ion diffusivity. In particular, the **GOP-PPF** provided in this work opens up a synthetic avenue for enhancing the doping of conjugated polymer-based electrodes operating in aqueous electrolytes.

To further investigate the redox behavior in aqueous media, the PMIECs' doping mechanism was studied by *in situ* UV-vis-NIR spectroelectrochemistry. We observed similar absorption spectra changes for all three PMIECs (Fig. S15, ESI†). First, a loss of intensity of the low energy absorption band (350–510 nm) and high energy band (510–1000 nm) was observed at potentials between −0.3 V and 0.7 V *vs.* Ag/AgCl. Specifically, upon gradually raising the applied bias up to 0.7 V, a new absorption feature around 1050 nm concomitantly increased, which was attributed to the formation of polarons.[17] Inversion of the potential to −0.3 V was employed to test the reversibility of the doping process. The optical signature of the polymers was fully restored in aqueous media, suggesting that these PMIECs have potential for electrochromic display applications.

2.4 OECT performance

An important application of mixed conduction materials is in OECT devices. OECTs operate as amplifying transducers, converting small changes in the gate voltage into large changes in the channel current, with an efficiency given by the transconductance, g_m, which is expressed as eqn (4):[46]

$$g_m = \frac{Wd}{L}\mu C^*(V_{th} - V_G) \quad (4)$$

The transconductance depends on the volumetric capacitance (C^*) and the charge mobility (μ) of the channel materials, as well as the channel thickness (d), length (L) and width (W), the gate voltage (V_G), and the threshold voltage (V_{th}). Typically, the μC^* value is the key parameter for evaluating the mixed conduction properties of the channel material in OECTs.[48] To investigate the role of EG composition in the mixed

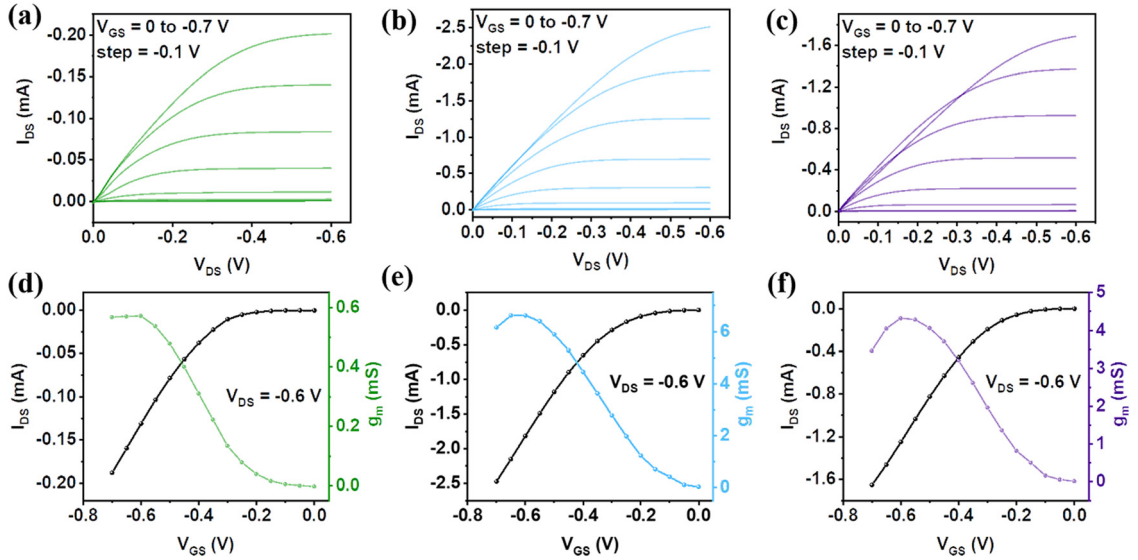

Fig. 4 (a, d), (b, e) and (c, f) Output curves, and transfer and transconductance characteristics for **g2T2-gBT2**, **g2T2-gBT4** and **g2T2-gBT6**-based OECTs, respectively.

Table 2 Characteristics of OECTs

Polymers	d [nm]	$g_{m,norm}$[a] [S cm^{-1}]	$I_{on/off}$	V_{th}[b] [V]	μ[c] [cm^2 V^{-1} s^{-1}]	C^*[d] [F cm^{-3}]	μC^*[e] [F V^{-1} cm^{-1} s^{-1}]	τ_{on} [ms]	τ_{off} [ms]
g2T2-gBT2	35 ± 3	16.3 ± 0.7	~10^3	−0.17	0.18	224	40	93	9
g2T2-gBT4	42 ± 3	154.9 ± 6.3	~10^3	−0.10	0.99	364	359	50	9
g2T2-gBT6	46 ± 4	92.4 ± 3.5	~10^3	−0.10	0.47	435	203	37	9

[a] The normalized average transconductance values. [b] Values determined by extrapolating the corresponding $I_{DS}^{1/2}$–V_{GS} plots. [c] Data obtained from the μC^* and the volumetric capacitance C^*. [d] Data deduced from EIS plots fit to an R_s ($R_p \| C$) circuit. [e] Data calculated from the equation: $g_m = WdL^{-1}\mu C^*(V_{th} - V_G)$.

ionic–electronic transport, the three PMIECs were studied as channel materials by fabricating OECTs. The output and transfer characteristics of the OECTs are shown in Fig. 4 and the corresponding data are summarized in Table 2.

OECTs fabricated using **g2T2-gBT4** reached a maximum drain current of 2.50 mA, much higher than 1.7 mA for **g2T2-gBT6** and nearly 14 times higher than 0.18 mA for **g2T2-gBT2** at the same $V_D = -0.6$ V (V_G set at −0.7 V) (see Fig. 4a–c). Similar trends in the normalized transconductance $g_{m,norm}$ were observed in the polymer series (Fig. 4d–f). **g2T2-gBT2** displayed the lowest $g_{m,norm}$ due to the combined effects of a low μC^* (40 F cm^{-1} V^{-1} s^{-1}, Fig. S16, ESI†) and a large threshold voltage ($V_{th} = -0.17$ V, Fig. S17, ESI†). As reported, the poor mixed conduction of **g2T2-gBT2** is likely due to low degree of swelling and ionic conduction, which increases the voltage required to oxidize the polymer.[49] Next, the $g_{m,norm}$ increased as the EG side chain length was increased, and **g2T2-gBT4** gave the highest $g_{m,norm}$ value (161.2 S cm^{-1}) among the three PMIECs, resulting from the significant improvement in the μC^* product (359 F cm^{-1} V^{-1} s^{-1}) as well as a decrease in V_{th} (−0.10 V). Further grafting longer EG side chains in **g2T2-gBT6**, however, resulted in a lower μC^* (203 F cm^{-1} V^{-1} s^{-1}) and decreased transconductance (95.9 S cm^{-1}).

To understand the volumetric doping process of the three copolymers, the electrochemical impedance spectroscopy (EIS) technique was used (Fig. S18, ESI†). The D_{Cl}^- can be calculated from Nyquist and Bode plots (see Fig. S18 a, b and e, ESI†) at low frequency, which corresponds to diffusion behavior of Cl^-.[50,51] In particular, the D_{Cl}^- is calculated with a value of 3.89 × 10^{-11} cm^2 s^{-1}, 1.68 × 10^{-10} cm^2 s^{-1} and 6.06 × 10^{-10} cm^2 s^{-1} for **g2T2-gBT2**, **g2T2-gBT4** and **g2T2-gBT6**, respectively, which is consistent with the values obtained from CV measurement (see Fig. 3). The volumetric capacitance (C^*) systemically increased as the side chain length was increased (check Fig. S18 c and d, ESI†), in agreement with the charge-storage capacity measurements. Furthermore, based on the μC^* and C^* values, the charge mobility (μ) can be obtained. Note that the calculated μ value (0.99 cm^2 V^{-1} s^{-1}) of **g2T2-gBT4** is the highest among the three copolymers. As reported, the introduction of EG side chains can facilitate ion transport in aqueous media, while some studies also pointed out that too much EG content would likely result in excessive water uptake during the electrochemical doping, disrupting the molecular crystallinity and reducing charge transport in some cases.[6,18] In this case, the highest μC^* was obtained for **g2T2-gBT4** as it maintained a balance between electronic charges and hydrated ion transport to maximize the mixed conduction in aqueous media.

From the transient behavior in Fig. S19 (ESI†), the turn on time (τ_{ON}) systematically decreased as the EG length increased, whereas the turn-off (τ_{OFF}) was unaffected. Note that the OECT

transient kinetics agree well with ion diffusion measurement results as the fastest doping speed was found for **g2T2-gBT6**. Additionally, the asymmetry in the switching characteristics between the τ_{ON} and τ_{OFF} was observed, which indicates the presence of a dissipation process, such as a viscoelastic component in the conducting pathway through the channel.[52] The on-to-off current ratios measured are on the same order of 10^3, comparable to the state-of-the-art OECTs.[20,48] Long term on–off switching performances were also carried out to test the stability of the OECTs operating in aqueous electrolytes. Note that three PMIECs presented similar operation stability of around 46% for 30 min (Fig. S20, ESI†).

2.5 Microstructure study

To analyze the microstructural features of the polymer films upon electrochemical doping, we collected *ex situ* grazing incidence wide-angle X-ray scattering (GIWAXS) of the films in their oxidized condition (doped at +0.7 V *vs.* Ag/AgCl in 0.1 M NaCl solution) (see Fig. 5 and Table S2, ESI†). Evidenced by the pronounced π–π scattering (010) from the in-plane direction, a predominant edge-on orientation was observed for all EG functionalized PMIECs. The three PMIECs exhibited a significant in-plane (010) peak at q_{xy} = 1.631, 1.648 and 1.620 Å^{-1} corresponding to a π–π spacing of 3.85 Å, 3.81 Å and 3.88 Å for **g2T2-gBT2**, **g2T2-gBT4** and **g2T2-gBT6**, respectively. Similarly, a shorter π–π stacking spacing was also found in **g2T2-gBT4** than its two analogues in the out-of-plane (010) direction. In particular, the shortest π–π stacking spacing for **g2T2-gBT4** could contribute towards the charge transport,[53] which agrees well with the highest mobility observed in the OECT device. Scattering profiles exhibited a lamellar diffraction peak (100) along the in-plane/out-of-plane direction corresponding to a lamellar *d*-spacing of 16.06/16.02, 19.87/19.87 and 21.51/21.73 Å for **g2T2-gBT2**, **g2T2-gBT4** and **g2T2-gBT6**, respectively. As we know, the lamellar stacking refers to the separation of the conjugated and aliphatic moieties.[54] With gradually raising the EG length, as expected, **g2T2-gBT6** exhibited the largest lamellar spacing due its longer linear side chain length.

Furthermore, *ex situ* atomic force microscopy (AFM) was applied to study the correlation between the EG composition and the morphology of the polymer films, and how the film morphology was affected by the injection of ions and water (Fig. S21, ESI†). In the pristine state, the three PMIECs exhibited similar root-mean square roughness (RMS) of 21.6 ± 0.1 nm. When the films were immersed in 0.1 M NaCl solution, the surface topographies of all polymer films appeared smoother with a reduced RMS value. The more even morphology in the hydrated state is indicative of a film swollen by ions and water.[16] Besides, after five CV cycles (−0.3 V to 0.7 V) in 0.1 M NaCl solution, a much rougher morphology was observed, with an increase in RMS value for all three PMIECs. Importantly, the rougher morphology was ascribed to ions and water penetration and exit cycles upon electrochemical doping and de-doping.[55] Notably, the most distinctive morphology change was found for **g2T2-gBT6**, which was consistent with electrochemical quartz crystal microbalance dissipation monitoring (EQCM-D) (*vide infra*).

2.6 EQCM-D measurement

To investigate the effects of EG composition on the swelling behavior upon electrochemical doping, we conducted EQCM-D measurement (Fig. S22, ESI†). In Fig. 6a, when the three PMIECs were immersed in 0.1 M NaCl solution, they displayed a similar passive swelling around 19.6%. However, a remarkable swelling change upon electrochemical doping at 0.7 V *vs.* Ag/AgCl was observed as the EG length progressively increases.

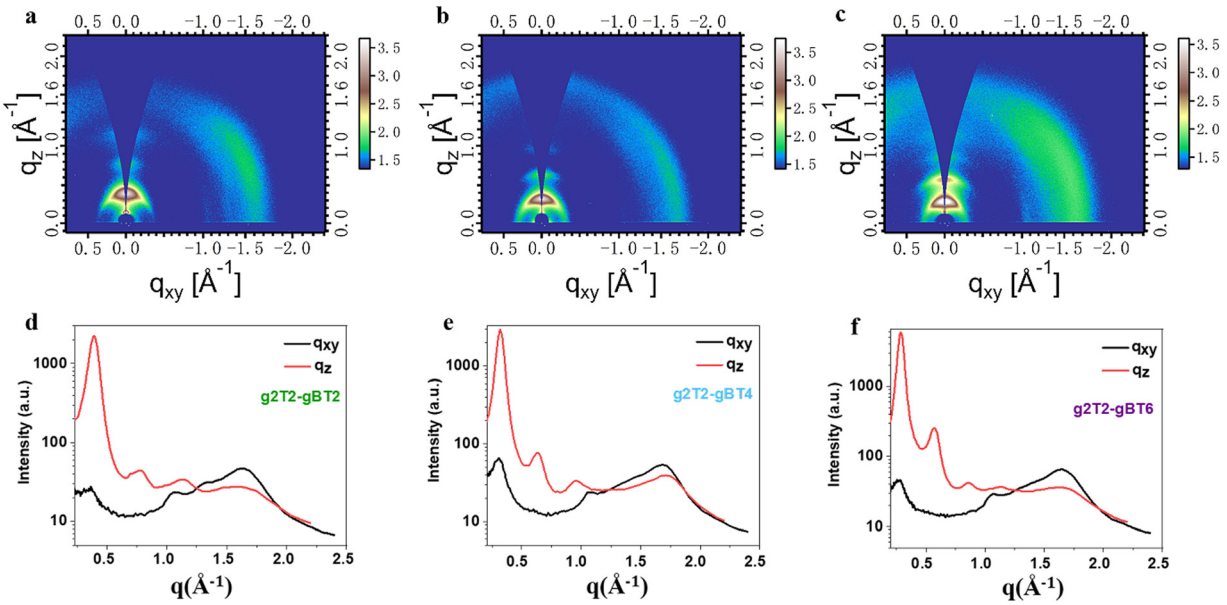

Fig. 5 GIWAXS patterns of the oxidized polymer films for (a and d) **g2T2-gBT2**, (b and e) **g2T2-gBT4** and (c and f) **g2T2-gBT6**, and corresponding line-cut profiles along the in-plane (q_{xy}) and out-of-plane (q_z) directions.

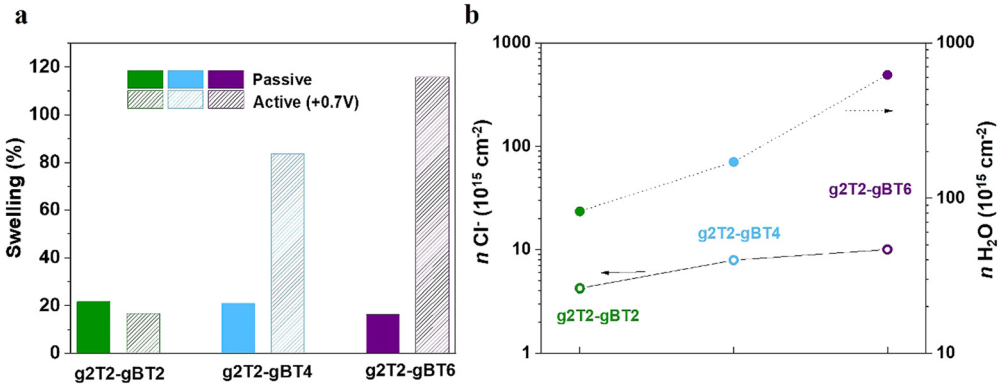

Fig. 6 (a) Polymer film swelling extent corresponding to the wet state with no potential bias (passive swelling) and electrochemical doping at +0.7 V *versus* Ag/AgCl (active swelling). (b) Concentration of Cl^- ions and H_2O molecule density in the polymer films oxidized at +0.7 V in aqueous solution.

In particular, an active swelling of 16.7% was found in **g2T2-gBT2**, followed by a significant increase to 83.6% for **g2T2-gBT4** and 115.7% for **g2T2-gBT6**. Notably, raising the EG content would contribute to the polymers swelling upon electrochemical doping in aqueous electrolyte, which was in agreement with previous studies.[56] As the active swelling of the polymers originated from the injection of ions and water, the specific amount of Cl^- ions and water molecules was calculated. As illustrated in Fig. 6b, all EG functionalized polymer films took more water than Cl^- ions during the doping process, with the ratios of H_2O/Cl^- uptake being 19.4, 21.6, and 62.1 for **g2T2-gBT2**, **g2T2-gBT4**, and **g2T2-gBT6**, respectively. This increasing Cl^- ion uptake with higher EG density trend is reflected in volumetric capacitance and energy storage measurements. In particular, the drop in charge mobility of **g2T2-gBT6** fabricated as an OECT was likely due to the molecular packing disruption as a result of excessive water uptake.[4,57,58] Furthermore, our results present that polymer swelling upon electrochemical biasing must be carefully balanced to avoid significant structural changes, which may reduce the electronic charge mobilities.

3. Conclusion

In this work, we established a new synthesis strategy, the **GOP-PPF** method, for largely expanding the synthesizable molecular design of PMIECs, toward incorporating a wide range of emerging functions. In particular, a series of PMIECs were prepared with varying EG composition by the **GOP-PPF** approach, which otherwise are highly time-consuming by conventional methods. We found that the EG length has little effect on the polymers' optical properties, while the hydrophilicity, redox behavior, ion diffusivity, charge storage and charge mobility in aqueous electrolytes were significantly influenced by EG length, as well as the performance in electrochemical devices. **g2T2-gBT6** exhibits the highest energy storage capacity exceeding 180 F g^{-1} among the three copolymers, which originates from the improved π-backbone doping, resulting in an ion-diffusivity increase. On the other hand, **g2T2-gBT4** gives the optimum balance of charge mobility and ionic–electronic coupling upon doping, exhibiting an impressive μC^* up to 359 F V^{-1} cm^{-1} s^{-1}. Importantly, optimizing the doping *via* tunable EG composition is crucial to maximize the performance of polymeric mixed conductors operating in aqueous media. Through innovative incorporation of a nucleophilic aromatic substitution reaction into the design and synthesis paradigm of high-performance PMIECs, we anticipate that this synthesis strategy will greatly enlarge the molecular design space and thus enrich the functional properties of PMIECs. Moreover, we believe that the **GOP-PPF** method proposed in this work will accelerate the development where ionic–electronic conduction is of paramount importance, including organic thermoelectrics, energy storage and electrochromics.

Author contributions

S. Cong synthesized the polymers and wrote the original manuscript; J. Chen carried out OECT measurements; B. Ding, Y. Wang, L. Lan and Z. Li provided helpful discussion; C. Chen coordinated the work; M. Heeney and W. Yue supervised the work; S. Cong prepared the manuscript with support from all co-authors; all authors discussed the results and contributed to this work.

Conflicts of interest

There are no conflicts of interest to declare.

Acknowledgements

S. Cong and J. Chen contributed equally to this work. The authors thank the National Natural Science Foundation of China (Grant No. 22275212), the Guangdong Basic and Applied Basic Research Foundation (Grant No. 2021A1515110261) and the Royal Society and Wolfson Foundation (Royal Society Wolfson Fellowship) for the financial support.

References

1 N. A. Kukhta, A. Marks and C. K. Luscombe, *Chem. Rev.*, 2021, **122**, 4325.

2 S. T. M. Tan, A. Gumyusenge, T. J. Quill, G. S. LeCroy, G. E. Bonacchini, I. Denti and A. Salleo, *Adv. Mater.*, 2022, **34**, 2110406.
3 S. Cong, J. Chen, L. Wang, L. Lan, Y. Wang, H. Dai, H. Liao, Y. Zhou, Y. Yu and J. Duan, *Adv. Funct. Mater.*, 2022, **32**, 2201821.
4 Y. He, N. A. Kukhta, A. Marks and C. K. Luscombe, *J. Mater. Chem. C*, 2022, **10**, 2314.
5 J. Chen, S. Cong, L. Wang, Y. Wang, L. Lan, C. Chen, Y. Zhou, Z. Li, I. McCulloch and W. Yue, *Mater. Horiz.*, 2023, **10**, 607.
6 N. A. Kukhta, A. Marks and C. K. Luscombe, *Chem. Rev.*, 2021, **122**, 4325.
7 B. D. Paulsen, K. Tybrandt, E. Stavrinidou and J. Rivnay, *Nat. Mater.*, 2020, **19**, 13.
8 Y. Wang, G. Zhu, E. Zeglio, T. C. H. Castillo, S. Haseena, M. K. Ravva, S. Cong, J. Chen, L. Lan and Z. Li, *Chem. Mater.*, 2023, **35**, 405.
9 X. Li, Y. Li, K. Sarang, J. Lutkenhaus and R. Verduzco, *Adv. Funct. Mater.*, 2021, **31**, 2009263.
10 P. R. Paudel, J. Tropp, V. Kaphle, J. D. Azoulay and B. Lüssem, *J. Mater. Chem. C*, 2021, **9**, 9761.
11 D. Ohayon, V. Druet and S. Inal, *Chem. Soc. Rev.*, 2023, **52**, 1001.
12 X.-X. Gao, D.-J. Xue, D. Gao, Q. Han, Q.-Q. Ge, J.-Y. Ma, J. Ding, W. Zhang, B. Zhang, Y. Feng, G. Yu and J.-S. Hu, *Sol. RRL*, 2019, **3**, 1800232.
13 M. Moser, L. R. Savagian, A. Savva, M. Matta, J. F. Ponder Jr, T. C. Hidalgo, D. Ohayon, R. Hallani, M. Reisjalali and A. Troisi, *Chem. Mater.*, 2020, **32**, 6618.
14 M. Moser, Y. Wang, T. C. Hidalgo, H. Liao, Y. Yu, J. Chen, J. Duan, F. Moruzzi, S. Griggs and A. Marks, *Mater. Horiz.*, 2022, **9**, 973.
15 P. Schmode, A. Savva, R. Kahl, D. Ohayon, F. Meichsner, O. Dolynchuk, T. Thurn-Albrecht, S. Inal and M. Thelakkat, *ACS Appl. Mater. Interfaces*, 2020, **12**, 13029.
16 A. Savva, R. Hallani, C. Cendra, J. Surgailis, T. C. Hidalgo, S. Wustoni, R. Sheelamanthula, X. Chen, M. Kirkus and A. Giovannitti, *Adv. Funct. Mater.*, 2020, **30**, 1907657.
17 L. Lan, J. Chen, Y. Wang, P. Li, Y. Yu, G. Zhu, Z. Li, T. Lei, W. Yue and I. McCulloch, *Chem. Mater.*, 2022, **34**, 1666.
18 M. Moser, L. R. Savagian, A. Savva, M. Matta, J. F. Ponder, T. C. Hidalgo, D. Ohayon, R. Hallani, M. Reisjalali, A. Troisi, A. Wadsworth, J. R. Reynolds, S. Inal and I. McCulloch, *Chem. Mater.*, 2020, **32**, 6618.
19 Y. Z. Wang, E. Zeglio, H. L. Liao, J. Q. Xu, F. Liu, Z. K. Li, I. P. Maria, D. Mawad, A. Herland, I. McCulloch and W. Yue, *Chem. Mater.*, 2019, **31**, 9797.
20 M. Moser, T. C. Hidalgo, J. Surgailis, J. Gladisch, S. Ghosh, R. Sheelamanthula, Q. Thiburce, A. Giovannitti, A. Salleo, N. Gasparini, A. Wadsworth, I. Zozoulenko, M. Berggren, E. Stavrinidou, S. Inal and I. McCulloch, *Adv. Mater.*, 2020, **32**, e2002748.
21 A. Giovannitti, C. B. Nielsen, D. T. Sbircea, S. Inal, M. Donahue, M. R. Niazi, D. A. Hanifi, A. Amassian, G. G. Malliaras, J. Rivnay and I. McCulloch, *Nat. Commun.*, 2016, **7**, 13066.
22 D. Ohayon, A. Savva, W. Du, B. D. Paulsen, I. Uguz, R. S. Ashraf, J. Rivnay, I. McCulloch and S. Inal, *ACS Appl. Mater. Interfaces*, 2021, **13**, 4253.
23 S. E. Chen, L. Q. Flagg, J. W. Onorato, L. J. Richter, J. Guo, C. K. Luscombe and D. S. Ginger, *J. Mater. Chem. A*, 2022, **10**, 10738.
24 H. Y. Wu, C. Y. Yang, Q. Li, N. B. Kolhe, X. Strakosas, M. A. Stoeckel, Z. Wu, W. Jin, M. Savvakis, R. Kroon, D. Tu, H. Y. Woo, M. Berggren, S. A. Jenekhe and S. Fabiano, *Adv. Mater.*, 2022, **34**, e2106235.
25 M. Rimmele, F. Glocklhofer and M. Heeney, *Mater. Horiz.*, 2022, **9**, 2678.
26 P. Li and T. Lei, *J. Polym. Sci.*, 2021, **60**, 377.
27 P. Schmode, A. Savva, R. Kahl, D. Ohayon, F. Meichsner, O. Dolynchuk, T. Thurn-Albrecht, S. Inal and M. Thelakkat, *ACS Appl. Mater. Interfaces*, 2020, **12**, 13029.
28 K. A. Günay, P. Theato and H.-A. Klok, *J. Polym. Sci., Part A: Polym. Chem.*, 2013, **51**, 1.
29 N. F. Konig, A. Al Ouahabi, S. Poyer, L. Charles and J. F. Lutz, *Angew. Chem., Int. Ed.*, 2017, **56**, 7297.
30 M. A. Gauthier, M. I. Gibson and H.-A. Klok, *Angew. Chem., Int. Ed.*, 2009, **48**, 48.
31 M. Raicopol, C. Andronescu, R. Atasiei, A. Hanganu and L. Pilan, *J. Electrochem. Soc.*, 2014, **161**, G103.
32 R. García-Loma and A. C. Albéniz, *RSC Adv.*, 2015, **5**, 70244.
33 E. Reichsollner, A. Creamer, S. Y. Cong, A. Casey, S. Eder, M. Heeney and F. Glocklhofer, *Front. Chem*, 2019, **7**, 123.
34 A. Creamer, C. S. Wood, P. D. Howes, A. Casey, S. Y. Cong, A. V. Marsh, R. Godin, J. Panidi, T. D. Anthopoulos, C. H. Burgess, T. M. Wu, Z. P. Fei, I. Hamilton, M. A. McLachlan, M. M. Stevens and M. Heeney, *Nat. Commun.*, 2018, **9**, 1.
35 J. Chen, Z. Yan, L. Tang, M. A. Uddin, J. Yu, X. Zhou, K. Yang, Y. Tang, T. J. Shin, H. Y. Woo and X. Guo, *Macromolecules*, 2018, **51**, 5352.
36 S. Cong, A. Creamer, Z. Fei, S. A. J. Hillman, C. Rapley, J. Nelson and M. Heeney, *Macromol. Biosci.*, 2020, **20**, 2000087.
37 Y. D. Park, D. H. Kim, Y. Jang, J. H. Cho, M. Hwang, H. S. Lee, J. A. Lim and K. Cho, *Org. Electron.*, 2006, **7**, 514.
38 J. K. Harris and E. L. Ratcliff, *J. Mater. Chem. C*, 2020, **8**, 13319.
39 Y. Wang, E. Zeglio, L. Wang, S. Cong, G. Zhu, H. Liao, J. Duan, Y. Zhou, Z. Li and D. Mawad, *Adv. Funct. Mater.*, 2022, **32**, 2111439.
40 A. Creamer, A. Casey, A. V. Marsh, M. Shahid, M. Gao and M. Heeney, *Macromolecules*, 2017, **50**, 2736.
41 C. Zhou, Y. Liang, F. Liu, C. Sun, X. Huang, Z. Xie, F. Huang, J. Roncali, T. P. Russell and Y. Cao, *Adv. Funct. Mater.*, 2014, **24**, 7538.
42 P. Li, J. Shi, Y. Lei, Z. Huang and T. Lei, *Nat. Commun.*, 2022, **13**, 5970.
43 K. Feng, W. Shan, S. Ma, Z. Wu, J. Chen, H. Guo, B. Liu, J. Wang, B. Li, H. Y. Woo, S. Fabiano, W. Huang and X. Guo, *Angew. Chem., Int. Ed.*, 2021, **60**, 24198.
44 S. Bhoyate, C. K. Ranaweera, C. Zhang, T. Morey, M. Hyatt, P. K. Kahol, M. Ghimire, S. R. Mishra and R. K. Gupta, *Glob. Chall.*, 2017, **1**, 1700063.
45 L. Q. Mai, A. Minhas-Khan, X. Tian, K. M. Hercule, Y. L. Zhao, X. Lin and X. Xu, *Nat. Commun.*, 2013, **4**, 2923.

46 B. Ding, G. Kim, Y. Kim, F. D. Eisner, E. Gutierrez-Fernandez, J. Martin, M. H. Yoon and M. Heeney, *Angew. Chem., Int. Ed.*, 2021, **60**, 19679.
47 M. Krajewski, B. Hamankiewicz, M. Michalska, M. Andrzejczuk, L. Lipinska and A. Czerwinski, *RSC Adv.*, 2017, **7**, 52151.
48 R. K. Hallani, B. D. Paulsen, A. J. Petty, R. Sheelamanthula, M. Moser, K. J. Thorley, W. Sohn, R. B. Rashid, A. Savva and S. Moro, *J. Am. Chem. Soc.*, 2021, **143**, 11007.
49 A. Giovannitti, D.-T. Sbircea, S. Inal, C. B. Nielsen, E. Bandiello, D. A. Hanifi, M. Sessolo, G. G. Malliaras, I. McCulloch and J. Rivnay, *Proc. Natl. Acad. Sci. U. S. A.*, 2016, **113**, 12017.
50 C. Gong, F. Deng, C.-P. Tsui, Z. Xue, Y. S. Ye, C.-Y. Tang, X. Zhou and X. Xie, *J. Mater. Chem. A*, 2014, **2**, 19315.
51 S. Zhang, J. Zhang, S. Xu, X. Yuan and B. He, *Electrochim. Acta*, 2013, **88**, 287.
52 J. T. Friedlein, M. J. Donahue, S. E. Shaheen, G. G. Malliaras and R. R. McLeod, *Adv. Mater.*, 2016, **28**, 8398.
53 Y. Wang, T. Hasegawa, H. Matsumoto and T. Michinobu, *J. Am. Chem. Soc.*, 2019, **141**, 3566.
54 Z.-F. Yao, J.-Y. Wang and J. Pei, *Cryst. Growth Des.*, 2017, **18**, 7.
55 Y. Wang, A. Hamidi-Sakr, J. Surgailis, Y. Zhou, H. Liao, J. Chen, G. Zhu, Z. Li, S. Inal and W. Yue, *J. Mater. Chem. C*, 2021, **9**, 13338.
56 A. Savva, R. Hallani, C. Cendra, J. Surgailis, T. C. Hidalgo, S. Wustoni, R. Sheelamanthula, X. X. Chen, M. Kirkus, A. Giovannitti, A. Salleo, I. McCulloch and S. Inal, *Adv. Funct. Mater.*, 2020, **30**, 1907657.
57 M. Moser, Y. Wang, T. C. Hidalgo, H. Liao, Y. Yu, J. Chen, J. Duan, F. Moruzzi, S. Griggs, A. Marks, N. Gasparini, A. Wadsworth, S. Inal, I. McCulloch and W. Yue, *Mater. Horiz.*, 2021, **9**, 973.
58 A. Savva, C. Cendra, A. Giugni, B. Torre, J. Surgailis, D. Ohayon, A. Giovannitti, I. McCulloch, E. Di Fabrizio, A. Salleo, J. Rivnay and S. Inal, *Chem. Mater.*, 2019, **31**, 927.

